

A Novel 3D-Bioprinting Technology of Orderly Extruded Multi-Materials via Photopolymerization

Jorge Alfonso Tavares-Negrete, Ceren Babayigit, Sahar Najafikoshnoo, Sang Won Lee, Ozdal Boyraz, and Rahim Esfandypour*

As a 3D bioprinting technique, digital light processing (DLP) has become popular due to its capability to provide high-throughput and high-resolution constructs with precise chemical and biological factor distributions. However, despite the advancements in DLP technology, several hurdles remain, including phototoxicity, extensive printing time, and the limited portfolio of biocompatible/photo-cross-linkable materials. Recently, few works have attended to resolve some of these issues. However, state-of-the-art techniques bear on complex imaging processing, require highly skilled personnel, and operate with non-biocompatible/photo-cross-linkable materials. Additionally, they are not yet capable of multi-layer and multi-material printing of biocompatible/photo-cross-linkable materials to fabricate physiologically relevant cell-laden structures. Herein, a novel DLP-based 3D-bioprinting technology called photopolymerization of orderly extruded multi-materials (POEM), is proposed, developed, and fully characterized. The utility of the POEM technique for rapid and high-resolution 3D-printing of multi-material, multi-layer, and cell-laden structures is demonstrated. The printed configurations show high cell viability ($\approx 80\%$) and metabolic activity for more than 5 days. As a study model, a 3D-structure representing the esophagus is also successfully printed and characterized. It is envisioned that the reported light-based POEM technique here enables the fabrication of 3D-cell-laden structures in a multi-material and multi-layer printing manner in biocompatible/photo-cross-linkable materials essential to construct complex heterogeneous tissues/organs.

1. Introduction

Bioprinting technology has rapidly advanced to provide a powerful platform to build anatomical and physiological relevant constructs.^[1] Previously, for more than the last 70 years, traditional two-dimensional (2D)^[2–8] approaches have been used in biomedical research (i.e., cell monolayers).^[5,9–11] However, these models have discrepancies, such as tissue heterogeneity and the poor recapitulation of human physiology, compared to an in vivo three-dimensional (3D) architecture (e.g., tissue-tissue interaction, vascularization, and cell communication).^[12,13] On the other hand, 3D-bioprinting offers unique spatial control over the 3D architecture of the biological components by combining hydrogels, cells, and signaling molecules to recreate actual tissues.^[14] Moreover, 3D-bioprinting contributes significant advances in drug screening,^[11,15–18] disease modeling,^[19,20] high throughput assays,^[21,22] cancer research,^[23,24] biofabrication,^[25–27] and clinical transplantation.^[28,29] In these regards, 3D-bioprinting technologies have been widely developed in tissue engineering and biomedical applications.^[30–32]

The foremost 3D-bioprinting technologies have been advanced with nozzle-^[33–36] and light-based techniques.^[37] The most common technique of nozzle-based bioprinting is extrusion

J. A. Tavares-Negrete, C. Babayigit, S. Najafikoshnoo, S. W. Lee, R. Esfandypour
Laboratory for Integrated Nano BioElectronics Innovation
The Henry Samueli School of Engineering
University of California
Irvine, CA 92697, USA
E-mail: rahimes@uci.edu

C. Babayigit, S. Najafikoshnoo, S. W. Lee, O. Boyraz, R. Esfandypour
Department of Electrical Engineering and Computer Science
University of California
Irvine, CA 92697, USA

J. A. Tavares-Negrete, R. Esfandypour
Department of Biomedical Engineering
University of California
Irvine, CA 92697, USA

J. A. Tavares-Negrete, C. Babayigit, S. Najafikoshnoo, O. Boyraz, R. Esfandypour
Henry Samueli School of Engineering
University of California
Irvine, CA 92697, USA

R. Esfandypour
Department of Mechanical and Aerospace Engineering
University of California Irvine
Irvine, CA 92697, USA

 The ORCID identification number(s) for the author(s) of this article can be found under <https://doi.org/10.1002/admt.202201926>

DOI: 10.1002/admt.202201926

bioprinting.^[38] The vat-photopolymerization techniques such as stereolithography,^[39] two-photon polymerization,^[40] and digital light processing (DLP)^[41,42] are categorized as the most frequently used light-based 3D-bioprinting technologies. Compared to the nozzle-based techniques, the light-based techniques provide more improved bioprinting resolution with smoother surfaces, fast printing speed, and high cell viability.^[43] Among the light-based technologies, the DLP has been more attention to 3D-bioprinting as a high-throughput technique with the capability to create high-resolution constructs with precise distributions of chemical and biological factors.^[44] However, DLP bioprinting has some hurdles, including irradiating photons from the light source leads to phototoxicity and DNA mutations. The extensive printing times stress the cells and increase the chances of contamination. Moreover, it has a limitation in the portfolio of photo-cross-linkable and biocompatible materials.^[45,46]

Recently, two DLP volumetric additive manufacturing techniques, including Xolography^[47] and, computed axial lithography (CAL)^[24] have attracted significant attention in light-based 3D-bioprinting technology.^[29,30] Both of these DLP techniques bear on the imaging processing part that requires complex operations, including skilled personnel and strong computational power.^[49] Nevertheless, the resins used in those works lack biocompatibility, precluding their translation to health applications.^[28,32] Furthermore, the current configuration of the resin reservoirs makes the volumetric printing of multi-materials impossible.^[51] For these reasons, the patterning of cell-laden polymers has remained a challenge to be addressed in terms of material selection, light intensity, and printing conditions.^[48,50] Hence, a biocompatible, multi-material, and rapid 3D-bioprinting system is yet to be developed.

Here, we address all the aforementioned limitations and present the photopolymerization of orderly extruded multi-materials (POEM), a novel 3D-bioprinting technique, to print 3D multi-layer, multi-material and cell-laden tissue structures with high cell viability and good resolution. The proposed technique relies on the implementation of biocompatible, photo-cross-linkable, and customizable hydrogels for rapid printing of multi-material and complex physiological relevant *in vivo* mimicking structures. The POEM technique principle of working is extrusion bioprinting of photo-cross-linkable hydrogels in a layer-by-layer manner followed by high-resolution patterning of the layers to the desired shapes and configurations using a 4-*f* lens system. The proposed POEM technique here maintains a high printing resolution, offers multi-material printing to achieve the heterogeneity presented in actual tissues and multicellular structures, eliminates cross-contamination and the cleaning process that is required in other state-of-the-art multi-material printing techniques, and enables multilayer printing to structurally mimic the *in vivo* tissue architectures. Moreover, the use of support bath implemented in the POEM technique holds the 3D-bioprinted structures still during the entire process and hence eliminates the chance of collision and any structural deformations.

Based on the POEM technique, sample 3D architectures (i.e., hexagonal ring, wheel, and cylinder structures) were successfully printed with a high resolution (65 μm) and analyzed by fluorescent imaging, indicating that the POEM enables printing along the *x*-, *y*-, and *z*-axis. The geometries were mimicked from the structure of the hepatic hexagonal lobule units, the intercon-

tion hepatic lobule-vasculature, and the esophagus multi-layered heterogeneity. Physiologically relevant esophagus models were bio-fabricated in a hollow tubular scale-down fashion to verify the POEM technique. To achieve biocompatibility, we used biomaterial formulations that are tailored according to the needs of cells to increase the survival rate, and to obtain non-toxic resins as opposed to previous works. In this context, a blend of poly(ethylene glycol) diacrylate (PEGDA) and gelatin methacryloyl (GelMA) polymers was designed to be photo-patterned and provided scaffolding to the muscle (C2C12) and fibroblast cells (L929). The esophagus-like structures maintain up to 80% cell viability and are metabolically active after printing and during the time (≈ 5 days), meaning that the POEM technique is suitable to be used in biomedical fields. Hence, the POEM technique paves the way for the 3D-bioprinting of multi-material and complex architectures closer to 3D-tissues with high resolution by using custom-made bioink formulations. With a custom selection of materials according to the application, it enables the printing of multi-material structures and the rapid bioprinting of cell-loaded structures with a simple post-processing routine.

2. Results and Discussion

2.1. The Design Approach and Principle of Operation

POEM technique can be separated into three main categories as preparation of the multi-material vats, patterning with the DLP system, and cleaning of the printing object as post-process (**Figure 1**). In the multi-material vat preparation part, it is required to place the various prepolymers (i.e., PEGDA or PEGDA+GelMA) in printer cartridges and neatly extrude them into the quartz reservoir (Figure 1a). Depending on the desired application, this extrusion process could be modeled in many configurations (e.g., longitudinal, lateral, etc.), applying different material thicknesses by tuning the printing speed, the needle gauge, and the G-code to the ink viscosity. The extrusion optimization will result in sharp boundaries between material layers. In contrast, the interconnection between multi-material layers resembles the anisotropic transition found in actual tissues. For example, the skin layers,^[52] bone-tendon junction,^[53] and gastrointestinal layers^[54] have intricate microscale anisotropic transitions. The complex hierarchical anisotropic topography directly impacts cell response by regulating their morphology, migration, and proliferation.^[55] To illustrate an optimized printing process, fluorescent particles with different colors were added to the prepolymer solutions. Then, they were extruded into longitudinal layers and concentric squares to generate lateral layering. In Figure 1a, the photographic view was given for the longitudinal layering case with three colors. For the patterning part, the proposed DLP-printing system consisted of i) an ultraviolet (UV) light source (395 nm, Darkbeam); ii) a digital micromirror device (DMD) chipset; iii) a computer to adjust and send the digital mask sequence; iv) optical projection lens system; and v) a stage for sample positioning, as illustrated in Figure 1b. In particular, the DMD chipset modulated the light by its 2D pixel arrays. From this modulation property, it has been deployed in many optical applications as a spatial light modulator to generate optical arbitrary waveforms,^[56,57] beam steerer for lidar applications,^[58,59] beam deflector for fast dispersive laser scanning systems.^[60,61] Here, the DMD chipset functioned as a

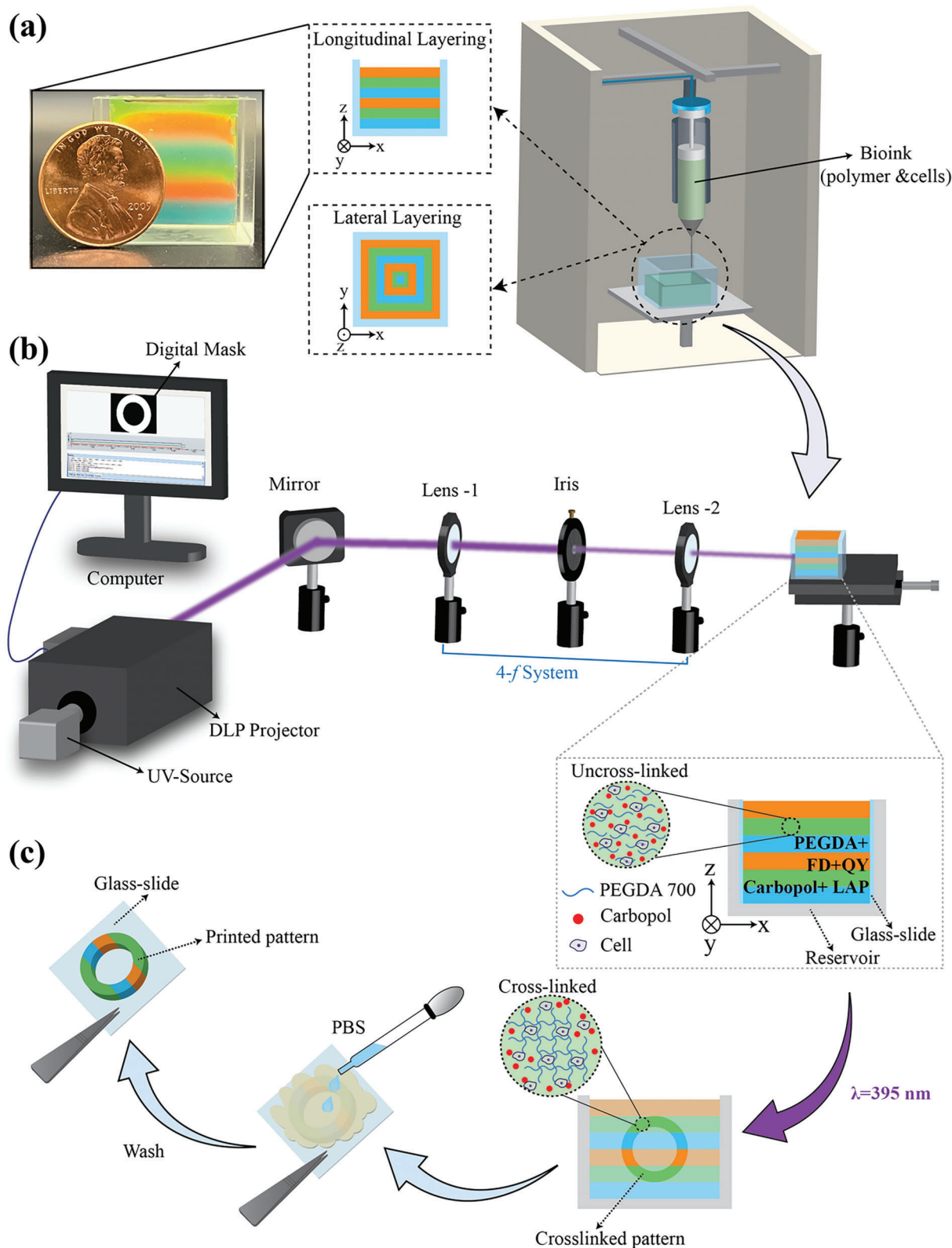


Figure 1. Schematic of the POEM technique printing configuration. a) Multilayer vat was prepared with extrusion printing as longitudinal or lateral layering configurations. The photographic view of the printed longitudinal layering case was presented with a coin to show the comparison of structural dimensions. b) The prepared vat was placed in the DLP printing system and exposed to patterned UV light ($\lambda = 395\text{ nm}$). c) After the crosslinking process, printed objects were removed from the vat and washed with PBS to clean the support bath on the printed object.

photomask to generate dynamic optical patterns.^[62] The DMD configuration with tilted mirrors has often been modeled as a blazed grating.^[63] Hence, the reflected beam from DMD contains some diffraction orders. It is important to retrieve in-focus images to be able to obtain sharp images which are directed to the bioink for the patterning process. For this retrieving process, a 4-*f* imaging system was introduced in our system to increase the image quality by introducing filtering at the Fourier plane. Moreover, one can introduce a resolution versatile-projection ratio, by changing the focal length of the lenses in the 4-*f* system.

For the 3D-bioprinting process, glass slides were placed against the inner walls of a quartz reservoir to remove the pattern without damaging it (Figure 1c). Then the reservoir was filled with prepolymer solution, which was composed of poly(ethylene glycol) diacrylate (PEGDA) 700 or a blend 2:1 of 20% PEGDA 700 and 10% gelatin methacryloyl (GelMA) as photo-cross-linkable polymers, Carbopol-940 as a viscose support bath, Lithium phenyl-2,4,6-trimethylbenzoylphosphinate (LAP) as biocompatible photo-initiator,^[64] and Quinoline yellow (QY) as photo-absorber. Once the DMD patterned UV light was projected on the reservoir, the exposed part of the prepolymer was crosslinked and converted into a solid polymer by a free polymerization reaction (Figure S1, Supporting Information). At the end of pattern illumination, the printed construct was firmly attached to the glass coverslip. As a post-printing process, a simple washing procedure was conducted by using phosphate-buffered saline (PBS) solution, after taking out the glass slide from the reservoir to remove the non-crosslinked material. In this way, the remaining Carbopol support bath (i.e., Carbopol-940) was depolymerized, and the non-crosslinked polymer was diluted. All the processes are summarized in Video S1, Supporting Information.

2.2. Printing of 3D Structures

We printed hexagonal ring, wheel, and cylinder structures to demonstrate the printing adaptability and applicability of the POEM technique (Figure 2). These three geometries were chosen to mimic the structure of the hepatic hexagonal lobule units,^[65] the interconnection hepatic lobule-vasculature,^[66,67] and the esophagus multi-layered heterogeneity,^[68,69] respectively. The hexagonal ring and wheel scaffolds with a single material were printed by using the two different digital masks (Figures 2a,d). Fluorescent particles were added to the prepolymer solution to obtain better visualized printed structures. The top and side views of the printed structures show that the details in the designed digital masks were successfully transferred to the printed scaffolds by single-step exposure for 3 min, as shown in Figure 2b,c,e,f. Each magnified microscope image indicated that the fluorescence particles were distributed homogeneously. Moreover, it showed that the POEM technique provided an appropriate resolution for printing the infills, and sharp inner/outer angles. The dimensions of the printed patterns were measured for comparison with the original design (Table 1). For each pattern, five samples were measured to determine the printing precision of the system. There was a negligible deviation (0.2–3.9%) between the measured and designed structural parameters, meaning a precision alignment and placement. The widths of the

printed structures were often higher than the designed values, due to a tiny over-curing. However, the slight differences between the measured and designed widths revealed that the proposed projection-based printing technique (i.e., POEM) has relatively acceptable accuracy and resolution.

Another point that should give attention is the thickness of the printed structures which is determined by the penetration depth of the light. The penetration depth is directed by many parameters, including the power of the light source, exposure time, the concentration of the photo-absorber, and the photo-initiator.^[70,71] Here, since the used exposure time, the concentration of the photo-absorber, and the photo-initiator were fixed for both structures, and their effect was ignored for the curing depth. The dominant factor was the power of the projected light. Note that the projected mask was composed of pixels and for each pixel, the light intensity was uniformly distributed. The total power for the curing was determined by the number of ON pixels in the digital mask, in other words, the area of the pattern. For the hexagonal ring pattern, the area was around $2.1873e^6$ pixels square. For the wheel pattern, since it was composed of multiple parts, one can use the most dominant part for the evaluation. The covered area was around $6.0078e^5$ pixels square, considering the outer ring as the dominant part. Therefore, it was expected that the hexagonal ring pattern would be a thicker structure. Besides, it was not possible to state a direct relationship between the pixel number and the thickness for the given structures due to the fact that different colors of fluorescent molecules were used for them. The reason was that the light intensity was determined by the absorption and scattering characteristics of the material, so not only these parameters but also the effect of the stray beams should be considered to make the relation. Apart from that, one could manipulate the thickness of the printed structure by controlling the number of ON/OFF mirrors.

As a next step, the multi-material structures were obtained by orderly extruding the multiple prepolymer solutions into the quartz reservoir via extrusion printing and then photocrosslinking in the DLP system. Through the POEM technique, an unrestricted number of inks/materials with multiple distribution configurations might be extruded to accommodate complex architectures. For the proof of concept, we have evaluated two printing scenarios. First, three multiple inks with colors of blue, green, and red were ordered in longitudinal configuration to assess two different geometries, cylindrical and gear shapes (Figure 1). The top view of the printed cylinder structure can be seen in Figure 2g. Then, two inks with blue and red colors were composed to arrange the lateral layering case (Figures 1 and 2h). To confirm the color transition between the layers, fluorescent microscope images were given for both lateral and longitudinal arrangements (Figure 2i–k). The influence of multi-material printing on the accuracy and resolution of the final structure is also examined by using two different materials in longitudinal layering arrangement and a mask that has vertical and horizontal symmetry, including circular, strip, and corner features, as shown in Figure S2, Supporting Information. The deviation between the measured and designed structural parameters is around 1.56–4.86% (Table S1, Supporting Information). However, the deviation between the two materials is around 0.1–0.4%, which shows that with a proper exposure time arrangement, one can get high accuracy with multi-material printing.

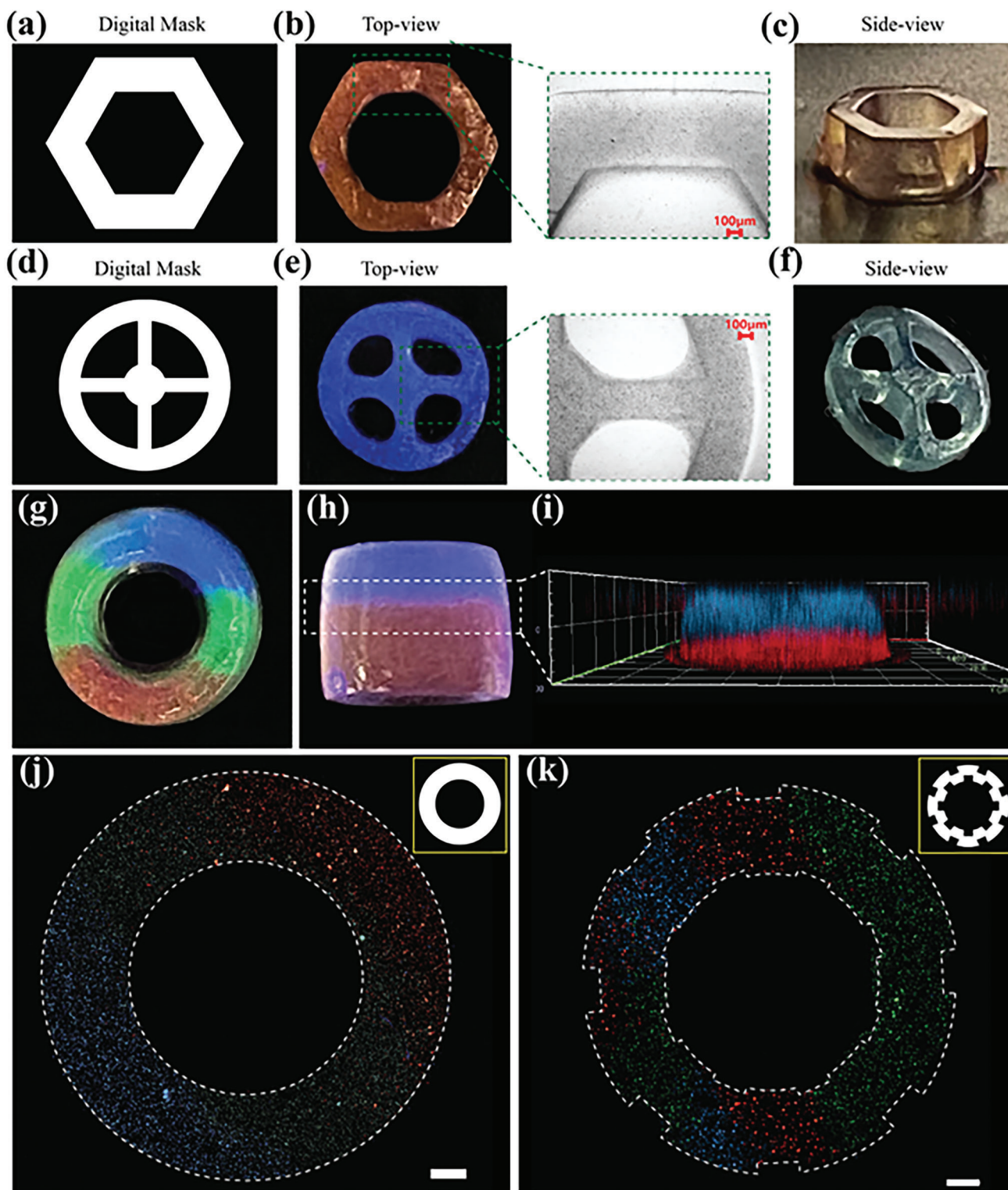
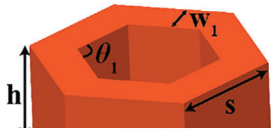
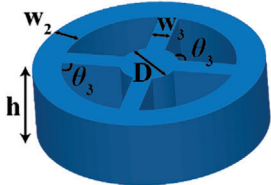


Figure 2. The application of POEM technique for the fabrication of multi-material structures. a) Digital mask for hexagonal ring pattern. b) Top view and c) side view of the DLP printed pattern for the hexagonal ring. The enlarged microscope image of the printed pattern was given as an inset in (b). d) Digital mask for wheel pattern. e) Top view and f) side view of the DLP printed pattern for the wheel. The enlarged microscope image of the printed pattern was given as an inset in (e). g) Top view of a DLP printed cylinder with longitudinal layering arrangement with three colors. h) Side view of a DLP printed cylinder with lateral layering arrangement. i) z-stack imaging of the cylinder in lateral layering configuration with two colors. Fluorescent microscope images of multi-material printed constructs with j) cylinder and k) gear patterns in longitudinal layering arrangement with three colors (scale bar = 500 μm). The used digital masks were depicted as an inset of each image. Here all the presented structures are printed with single-step exposure.

Table 1. The dimensions of original designs and DLP printed patterns ($n = 5$) ($w_1/w_2/w_3$: width, s : side, h : height, D : diameter, and $\theta_1/\theta_2/\theta_3$: corner angle).

Patterns	Dimensions [mm]			
	Original design	Printed structure	Percent error	
	w_1	1.00	1.002 ± 0.021	0.2%
	s	2.89	2.777 ± 0.031	3.9%
	h	N.A.	2.040 ± 0.016	N.A.
	θ_1	120°	122.786 ± 0.032	2.3%
	D	1.25	1.272 ± 0.013	1.76%
	w_2	0.62	0.633 ± 0.008	2.1%
	w_3	0.42	0.436 ± 0.006	3.8%
	h	N.A.	1.566 ± 0.02	N.A.
	θ_2	82°	79.462 ± 0.079	3.1%
	θ_3	111°	111.982 ± 0.081	0.9%

2.3. Bioprinting

The POEM technique has the potential to offer a biocompatible environment to incorporate living cells in the bioprinting process. Although light damage to DNA and radicals are beyond the scope of this paper, the biocompatibility of the POEM technique, the polymers (i.e., PEGDA 700 and GelMA), and the support bath (i.e., Carbopol-940) were investigated, we printed esophagus-like structures as a model by incorporating muscle cells (C2C12) and fibroblast cells (L929) into the PEGDA (i.e., PEGDA 700) and PEGDA+GelMA inks.^[72] We have investigated the cell viability in the polymeric bioinks through the Live/Dead assay (Figure 3a). The Live/Dead assay showed a large population of viable cells on the first day of printing $91.2 \pm 3.5\%$ and $68.5 \pm 6.0\%$ for PEGDA+GelMA and PEGDA, respectively (Figure 3b). Nonetheless, a preserved cell viability of up to 80% was observed on day 5 for the PEGDA+GelMA blend. Besides, up to a 25% of reduction in cell viability was observed for PEGDA ink for 5 days (Figure 3b). Life and dead assay confirmed significantly higher cell viability in the PEGDA+GelMA blend ($^{***}p$ -value ≤ 0.001). Moreover, this tendency was confirmed by the Resazurin assay. In Figure 3c, the bar graphs showed that the metabolic activity on day 5 decreased up to 60% in PEGDA ink, while in PEGDA+GelMA the variation was $\approx 25\%$ in comparison with metabolic activity on day 1, which is similar to the previous works.^[39,73] The reduction of cell viability in hydrogels of PEGDA might be attributed to the pore size of PEGDA which was too small to allow the medium diffusing.^[39] The pore size of PEGDA also affects the stiffness of the material and the mechanotransduction of the cells.^[74] The mechanical properties of PEGDA can be tuned by adding other photo-cross-linkable polymers like GelMA. The use of PEGDA with higher molecular weight may result in larger pores improving cell viability.^[75,76] As well, the formulation of photo-crosslinkable bioinks with natural-origin polymers and supplemented with additives (i.e., RGD particles, dECM, FGF, FBS) may improve the cell function and expand the bioink portfolio. The use of support baths with degradable polymers like poly(ethylene glycol) or poly(D, L-lactide) can be po-

tentially applied in the POEM technique to generate implantable constructs.

2.4. Characterization of the Photo-Cross-Linkable System

The performance of the proposed POEM system was characterized by evaluating its resolution and registration capability with respect to the exposure time (0.5–3 min). To optimize the exposure time for target thickness, the PEGDA prepolymer solution was patterned, varying the exposure times for different strip thicknesses (65–2000 μm). The minimum width of the strips was designed considering that in bioprinting, high resolution is defined as printed elements smaller than 100 μm since it is comparable to the size of a single cell.^[77] Nonetheless, the limit range of strip thickness was stated previously, since the photo-crosslinking is controlled by the pixel number, the wider thicknesses are crosslinked in a shorter exposure time (Figure 4a). Here, the exposure time was limited to 3 min. by considering the cell viability at the bioprinting part.^[42] The printing resolution featured up to 65 μm with the proposed POEM technique. Another considerable point is the engineering of the exposure time by superimposing digital masks to compound different feature sizes on a macrostructure. Figure 4b showed the procedure of a basic case study for the superimposition of the masks. For the exposure time versus printing resolution, it was sufficient for the printing strip with 65 μm thickness with 3 min. of exposure time, and 45 s for a 2000 μm feature size. Hence, to avoid over-crosslinking of the wider part, a mask that only contained the thinner strip was projected on the polymer. Then, the wider pattern was superimposed at the target time (i.e., 2:25 min.). As shown in the presented bright field microscopy image, the strips were printed with designed thicknesses with the superimposition of the masks at proper times (Figure 4b).

For the extrusion of inks, the rheology properties of the materials determine their feasibility to be extruded and keep the shape after the material is released from the hydraulic pressure. We have conducted a rheology characterization of all the materials; Carbopol, PEGDA prepolymer, PEGDA-Carbopol, PEGDA+GelMA, and PEGDA+GelMA-Carbopol (Figure 4c). All the materials showed a shear-thinning behavior, meaning that their viscosity decreases with increasing shear rates. This confirms their capability to be implemented in 3D-extrusion-printing. The viscosities of the materials evaluated at the lowest shear rate were 0.91 ± 0.13 , 1.20 ± 0.02 , 21.66 ± 2.97 , 51.36 ± 1.60 , and 31.47 ± 2.51 Pa·s for PEGDA prepolymer, PEGDA+GelMA, PEGDA-Carbopol, Carbopol, and PEGDA+GelMA-Carbopol, respectively (Figure 4c). As expected, with the incorporation of the Carbopol support bath to PEGDA, the PEGDA+GelMA yields inks with higher viscosity while preserving the shear thinning behavior. The absorbance spectra of all materials were investigated (Figure 4d). First, the absorbance of Carbopol presented minimal interference with the light, due to its transparency and the absence of any impurity. Second, QY absorbs in the range between 360 and 475 nm, with its higher absorbance at 410 nm. The light absorption of QY was attenuated in combination with PEGDA, PEGDA+GelMA, and Carbopol, due to the dissolution of concentration. The swelling

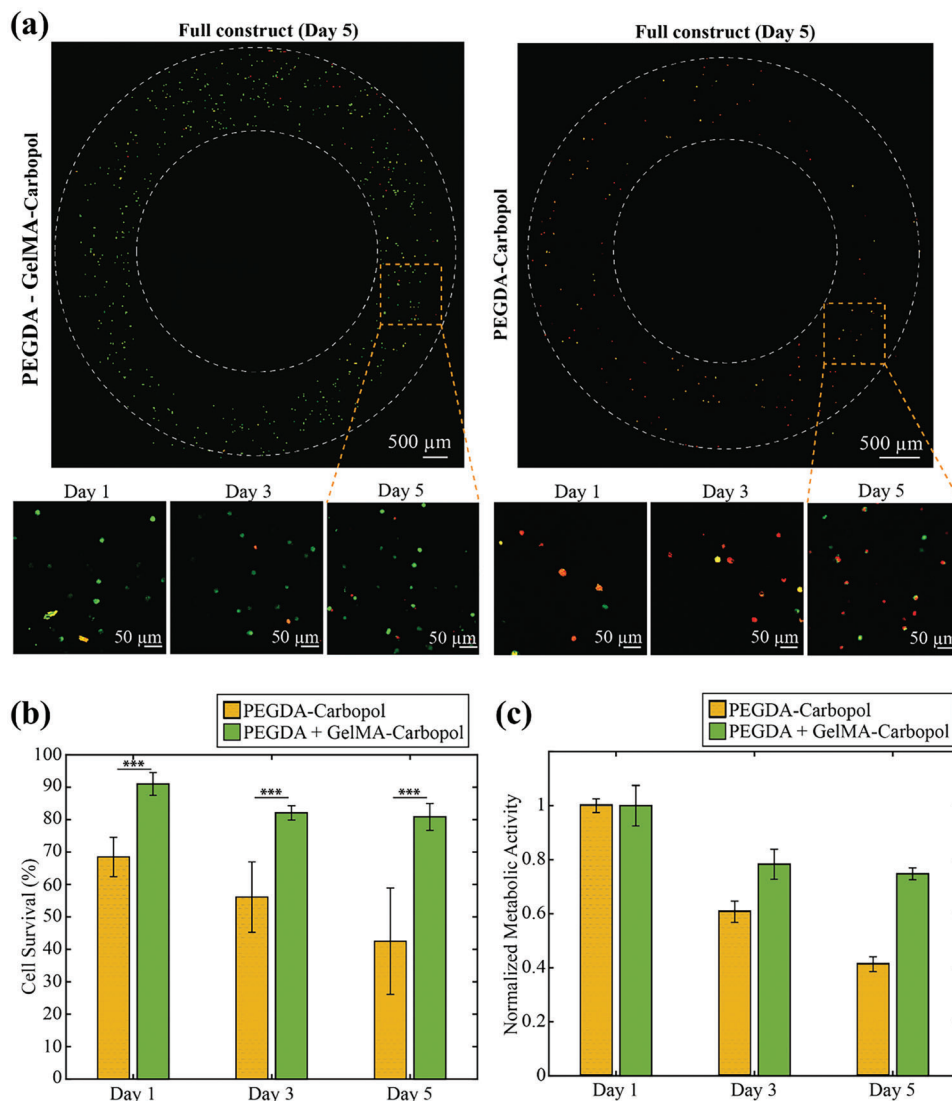


Figure 3. 3D cell-laden bioprinting experiments. a) Live/Dead assays of printed constructs of PEGDA and PEGDA+GelMA on days 1, 3, and 5, and image stitching of the full shape of constructs on day 5. b) Quantitative analysis of cell viability assay ($N = 3$, $n = 4$, $***p \leq 0.001$). c) Resazurin assay on cells encapsulated in bioprinted constructs ($N = 3$).

properties of a polymer network reflect its mechanical properties, diffusion capability, and surface mobility.^[78] The swelling behavior of PEGDA-Carbopol and PEGDA+GelMA-Carbopol xerogels showed a rapid swelling in the first 5 h achieving stable equilibrium in about 16 h. The water swelling increased with time, and the constructs increased their swelling ratio by $\approx 1500\%$ compared to their dry weight due to the water retention of PEGDA. This swelling behavior is similar to the one reported by other authors.^[79] The data demonstrated the ability of GelMA to reduce the swelling ratio in comparison with PEGDA-Carbopol. The mechanical properties of hydrogels affected cell proliferation and differentiation. Thus, it is important to measure the mechanical properties of the PEGDA-Carbopol and the PEGDA+GelMA-Carbopol. The compressive strength of the PEGDA-Carbopol (≈ 139.9 Pa) results was higher than PEGDA+GelMA-Carbopol (≈ 35.6 Pa), due to the rigidity of PEGDA chains.^[80] To elucidate

the changes in mechanical properties of single materials while applied to fabricate multi-material structures, hemispheres were printed and its behavior was tested under compression test (Figure S3, Supporting Information), assuming that if there is uniform crosslinking for the multi-material printing, the mechanical properties of the multi-material structure should show stiffness characteristics which is the average of the materials that compose it.^[81] Uniaxial compression showed differences in the mechanical properties of green- and orange-colored inks. Specifically, the average onset of fracture of green- and orange-colored inks are ≈ 32 and $\approx 55\%$, respectively. In contrast, the multi-material constructs displayed fracture points in compressive strains of $\approx 43\%$ between their individual components. To emulate the tissue mechanical properties, hydrogels might be tuned with the co-formulation of small molecular weight PEGDA and high molecular weight hydrogels like GelMA.

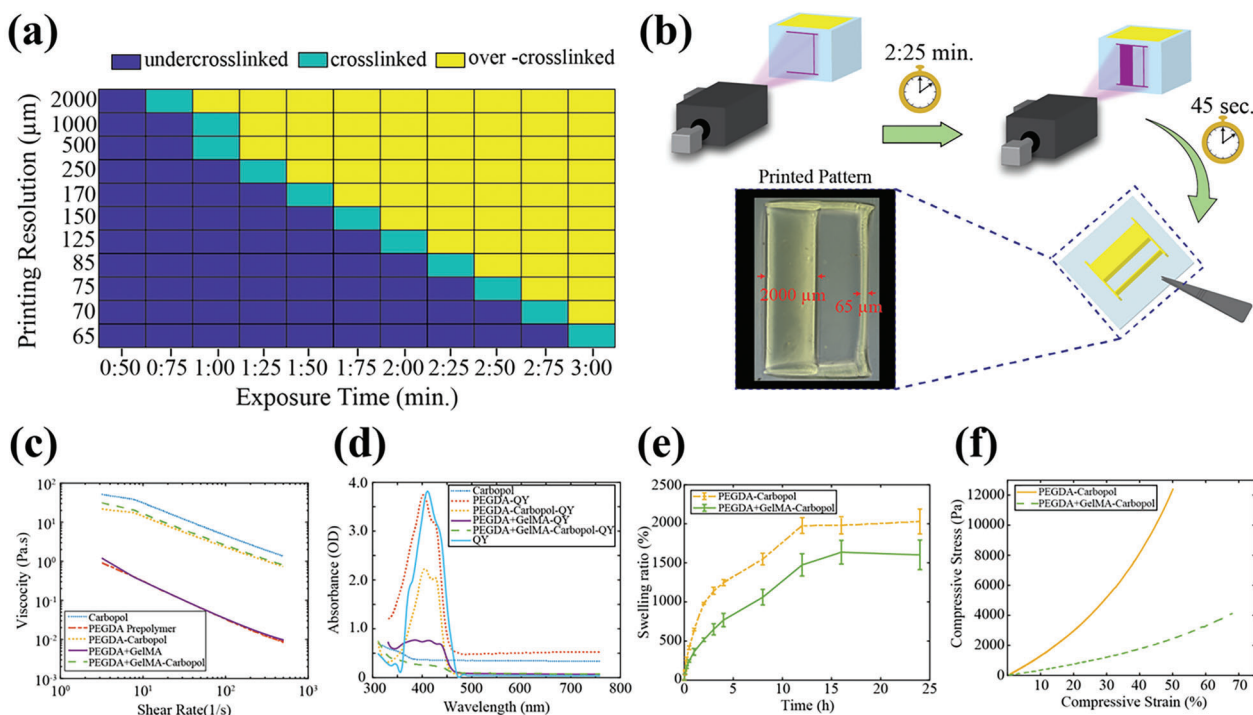


Figure 4. a) Resolution analyses of the system concerning the exposure time. b) Example for superposition of the masks at appropriate times to achieve high and low-resolution patterns in the same structure. c) Flow curve, d) absorption spectrum, e) water swelling characteristics, and f) mechanical properties of the materials.

3. Conclusion

State-of-the-art DLP techniques bear on complex imaging processing, require highly skilled personnel, operate with non-biocompatible/photo-cross-linkable materials, and are not yet capable of multi-layer and multi-material printing of biocompatible/photo-cross-linkable materials to fabricate physiologically relevant cell-laden structures. Herein, a novel DLP-based 3D-bioprinting technology is proposed, developed, and fully characterized. The POEM technique principle of working is extrusion bioprinting of photo-cross-linkable hydrogels in a layer-by-layer manner followed by high-resolution patterning of the layers to the desired shapes and configurations using a 4-f lens system. The utility of the POEM technique for rapid and high-resolution 3D-printing of multi-material, multi-layer, and cell-laden structures is demonstrated. The printed configurations showed high cell viability ($\approx 80\%$) and metabolic activity for more than 5 days. As a study model, a 3D structure representing the esophagus is also successfully printed and characterized. The proposed POEM technique here maintains a high printing resolution, offers multi-material printing to achieve the heterogeneity presented in actual tissues and multicellular structures, eliminates cross-contamination and the cleaning process that is required in other state-of-the-art multi-material printing techniques, and enables multilayer printing to structurally mimic the in vivo tissue architectures. Moreover, the use of support bath implemented in the POEM technique holds the 3D-bioprinted structures still during the entire process and hence eliminates the chance of collision and any structural deformations. We envision the proposed POEM technique shed light on a novel 3D-

bioprinting technique for the field of bioprinting multi-material and complex architectures mimicking in vivo 3D tissues with high resolution.

4. Experimental Section

Materials: Poly(ethylene glycol) diacrylate (PEGDA-700) Mn 700 and Quinoline Yellow (QY) were purchased from Sigma Aldrich, USA. Carbopol-940 was purchased from Acros Organics. Lithium phenyl-2,4,6-trimethyl-benzoyl phosphinate (LAP) was purchased from Allevi. DMEM media, ANTI-ANTI, and Fetal Bovine Serum were purchased from Gibco. The UV-395 nm torch was purchased from Darkbeam-Amazon. DLP Projector (DLP LightCommander) was purchased from Texas Instruments, USA. Lenses, iris, and mirrors were purchased from Thorlabs.

GelMA Synthesis: GelMA was synthesized by dissolving type A gelatin from porcine skin at 10% (w/v) in Dulbecco's phosphate-buffered saline (DPBS) and stirring at 50 °C and 300 rpm for an hour. Methacrylic acid was added dropwise with a syringe pump (0.3 mL min^{-1}) to the solution at 5% (v/v) and allowed to react for 1 h. The reaction was finished by adding 5x volumes of DPBS. The resulting solution was dialyzed for 7 days with distilled water (DW) at 37 °C. The resulting solution was frozen and lyophilized for 5 days and stored at -80 °C before use.

Preparation of PEGDA Ink: To prepare the prepolymer PEGDA inks, 20% w/v solution of PEGDA-700 was mixed with 0.1% w/v QY. Then, the PEGDA solution was heated at 65 °C for 20 min. This process was followed by the addition of 0.5% w/v LAP (ALEVY) photo-initiator and pH neutralization with NaOH (1 M). The PEGDA solutions were sterilized using 0.22 μm polyether sulfone (PES) filters, before being applied for 3D-bioprinting of the cells.

Preparation of GelMA Ink: Lyophilized GelMA was dissolved at 10% (w/v) in DW and mixed with 0.025% w/v QY, followed by the addition of 0.1% (w/v) of LAP as the photo-initiator and pH neutralization with NaOH (1 M). Finally, GelMA solutions were sterilized using 0.22 μm PES filters.

Preparation of Carbopol-Support Bath: According to the previous work,^[82,83] the synthesis of the Carbopol support bath was adapted to the POEM technique. Briefly, a 1.2% w/v solution of Carbopol-940 was prepared by vortex mixing in DW, then 0.5 mL of NaOH (1 M) was added. After that, the Carbopol support bath was mixed and centrifuged at 3000 rpm for 20 min.

Preparation of PEGDA-Support Bath: The PEGDA-Carbopol support bath was prepared by mixing 3 mL of PEGDA ink in 7.5 mL of the Carbopol-940 support bath.

Preparation of PEGDA+GelMA-Support Bath: The PEGDA+GelMA-Carbopol-940 support bath was prepared by mixing 1 mL of PEGDA ink with 2 mL of GelMA in 7.5 mL of the Carbopol-940 support bath.

Rheological Test: The rheological properties of prepolymer PEGDA ink, Carbopol support bath, and the mix of PEGDA-Carbopol were investigated by using a DHR rheometer (TA Instruments) equipped with a Peltier. A 20 mm parallel plate with a 200 μm gap was used for all rheological tests. PEGDA, Carbopol-940, and PEGDA-Carbopol mix were loaded, and their complex viscosity was studied as a function of shear rate (1–100 Hz) at 24 °C with a constant strain of 2% ($n = 3$).

Absorption Spectra of the Materials: Absorption spectra of the prepolymer PEGDA ink, Carbopol support bath, and the mix of PEGDA-Carbopol were measured by a UV-visible spectrophotometer Biotek Cytation 5/Biospa Plate Reader and the results were plotted as a function of wavelength in a range from 200–800 nm. Polymers were prepared as described previously, and a blank of DW was used.

Compressive Modulus: To test the mechanical properties, 5 mL of PEGDA-Carbopol solution was extruded into a 12-well plate and crosslinked at 395 nm with UV light for 60 s. Then the samples were taken off the well plate. Young's modulus was tested by a dynamic mechanical analysis instrument (Instron 3365 UTS). The compressive modulus was determined as the slope of the linear region between strains from 5 to 20%.

Hydrogel Swelling: For the measurement of water swelling, six cylindrical samples were prepared using the protocol described above. To leach the unreacted-soluble fraction, the samples were placed in water at room temperature for 24 h. Then samples were dried in a vacuum desiccator for 2 days. Next, the dried samples were immersed in DW at 37 °C. The swelling kinetics was studied after taking out the soaked samples from water at different time points and weighing them once the surface droplets were wiped off with wet paper until getting constant weight. The swelling ratio was determined by the following equation:

$$S_w (\%) = \frac{W_t - W_0}{W_0} \times 100$$

where W_t is the weight of the hydrogel sample at a specific time, and W_0 is the weight of the dried samples recorded as the initial weight. All experiments were performed in triplicate.

DLP Printing: Printing was performed by customizing the projection lens and illumination source of the commercial DLP (Texas Instruments, Dallas, TX). Instead of using its illumination module with a visible light source, a UV source operating at 395 nm was integrated for the illumination of the DMD (Texas Instruments, Dallas, TX) chips. The projection optics was replaced with a 4- f system and the optical path was adjusted with an $\times 0.7$ scaling by properly arranging the focal lengths of the lenses. The DMD chip in the system consists of 1024 \times 768 individually controllable micromirrors of 10.8 μm size. Hence, one pixel on a mask was reflected by one mirror on the DMD chip was about 7.56 \times 7.56 μm^2 after being projected from the 4- f system to the target pre-polymer. All digital masks were designed in Adobe Illustrator and loaded as BMP files into the projection software of the DLP printer.

A quartz reservoir was filled with the polymer + support bath (which functions as a holder for the printed structure) mixture, and a glass slide (size: 18 \times 18 mm) was placed in between the reservoir wall and the polymer to easily remove the printed pattern without damaging it. Then, the quartz reservoir was placed over the stage and the mask was projected against the reservoir wall.

POEM: First, the polymers+support bath was transferred into cartridges and degassed by centrifugation at 2000 rpm for 10 min.; subsequently, cartridges were loaded in the 3D-extrusion-bioprimer (Incredible+, Cellink, Sweden). Then the G-code to fill the reservoir in the desired pattern was uploaded. The materials were orderly extruded inside the quartz reservoir using 14 G needles, and the final product was covered with parafilm.

Printing Resolution: To evaluate the printing resolution of the system, a calibration structure consisting of an array of strip features of decreasing size and gaps were printed. After recovering the samples, the fidelity of printed structures was evaluated by using image analysis. Photographic images of printed structures were analyzed using Toupview software (AmScope, USA) and compared to the original design parameters ($n = 3$).

Cell Culture: Mouse fibroblast C2C12 was kindly provided by Professor Masashi Kitazawa from the UC Irvine School of Medicine, and mouse myoblast L929 kindly provided by Professor Angela G. Fleischman from UCI School of Medicine was used for this study. Bout cell lines were cultured in an incubator at 37 °C under a 5% CO₂ atmosphere. The standard cell culture media was made from Dulbecco's Modified Eagle Medium (DMEM) supplemented with 10% of fetal bovine serum and 1% of Anti-Anti.

Cell Viability Assay: Cell viability test of L929 and C212 proceeded on days 1, 3, and 5 by performing a LIVE/DEAD assay (Life Technologies, California, United States) which contained 2 mM calcein-AM and 4 mM ethidium homodimer (EtHD1). The samples were placed in a dark humidity incubator for 30 min. Then constructs were washed with PBS and immediately imaged using The Zeiss LSM 900 Airyscan 2 confocal fluorescence microscope (Zeiss, Germany).

Metabolic Activity Analyses: Metabolic activity was accessed on days 1, 3, and 5 using the Reassuring assay (Biotium, USA). Briefly, constructs were covered in DMEM culture media with 10% v/v Reassuring reagent and incubated for 2 h at 37 °C. After incubation in a 96-well plate, 100 μL of media were transferred, and the fluorescence was measured in a microplate reader at 530/571 nm excitation/emission wavelengths. Fluorescence readings were normalized with respect to control well with the medium in the absence of biological samples.

Statistical Analysis: Analysis of variance was performed with SPSS 27 (IBM, USA). Differences with a p -value < 0.001 (***) were considered statistically significant.

Supporting Information

Supporting Information is available from the Wiley Online Library or from the author.

Acknowledgements

J.A.T.-N. and C.B. contributed equally to this work.

Conflict of Interest

The authors declare no conflict of interest.

Data Availability Statement

The data that support the findings of this study are available upon reasonable request.

Keywords

3D-bioprinting, biomaterials, digital light processing, multi-material, photopolymerization, photopolymerization of orderly extruded multi-materials

Received: December 11, 2022
Revised: February 11, 2023
Published online: April 4, 2023

- [1] I. T. Ozbolat, K. K. Moncal, H. Gudapati, *Addit. Manuf.* **2017**, *13*, 179.
- [2] R. Esfandyarpour, H. Esfandyarpour, M. Javanmard, J. S. Harris, R. W. Davis, *Sens. Actuators, B* **2013**, *177*, 848.
- [3] R. Esfandyarpour, M. Javanmard, Z. Koochak, H. Esfandyarpour, J. S. Harris, R. W. Davis, *Biomicrofluidics* **2013**, *7*, 044114.
- [4] R. Esfandyarpour, M. Javanmard, Z. Koochak, J. S. Harris, R. W. Davis, *2014 IEEE 27th International Conference on Micro Electro Mechanical Systems (MEMS)*, IEEE, San Francisco, CA **2014**, pp. 1083–1086.
- [5] R. Esfandyarpour, M. Javanmard, Z. Koochak, J. S. Harris, R. W. Davis, *Biotechnol. Bioeng.* **2014**, *111*, 1161.
- [6] R. Esfandyarpour, Z. Koochak, J. S. Harris, R. W. Davis, *2015 Transducers –2015 18th International Conference on Solid-State Sensors, Actuators and Microsystems (TRANSDUCERS)*, IEEE, Anchorage, AK **2015**, pp. 1523–1526.
- [7] R. Esfandyarpour, H. Esfandyarpour, M. Javanmard, J. S. Harris, R. W. Davis, *MRS Online Proc. Libr.* **2012**, *1414*, mrsf11.
- [8] S. Kumar, R. Esfandyarpour, R. Davis, Y. Nishi, *J. Appl. Phys.* **2014**, *116*, 074511.
- [9] H. Eagle, G. E. Foley, *Cancer Res.* **1958**, *18*, 1017.
- [10] V. Velasco, S. A. Shariati, R. Esfandyarpour, *Microsyst. Nanoeng.* **2020**, *6*, 76.
- [11] R. Mazrouei, V. Velasco, R. Esfandyarpour, *Sci. Rep.* **2020**, *10*, 14669.
- [12] B. Byambaa, N. Annabi, K. Yue, G. Trujillo-de Santiago, M. M. Alvarez, W. Jia, M. Kazemzadeh-Narbat, S. R. Shin, A. Tamayol, A. Khademhosseini, *Adv. Healthcare Mater.* **2017**, *6*, 1700015.
- [13] K. A. Gold, B. Saha, N. K. Rajeeva Pandian, B. K. Walther, J. A. Palma, J. Jo, J. P. Cooke, A. Jain, A. K. Gaharwar, *Adv. Healthcare Mater.* **2021**, *10*, 2101141.
- [14] J. L. Albritton, J. S. Miller, *Dis. Models Mech.* **2017**, *10*, 3.
- [15] W. Peng, P. Datta, B. Ayan, V. Ozbolat, D. Sosnoski, I. T. Ozbolat, *Acta Biomater.* **2017**, *57*, 26.
- [16] J.-Z. Wang, N.-Y. Xiong, L.-Z. Zhao, J.-T. Hu, D.-C. Kong, J.-Y. Yuan, *Int. J. Surg.* **2018**, *56*, 1.
- [17] V. Velasco, K. Joshi, J. Chen, R. Esfandyarpour, *Anal. Chem.* **2019**, *91*, 14927.
- [18] M. I. Vanegas, K. R. Hubbard, R. Esfandyarpour, B. Noudoost, *J. Visualized Exp.* **2019**, *153*, 60365.
- [19] A. Memic, A. Navaei, B. Mirani, J. A. V. Cordova, M. Aldahri, A. Dolatshahi-Pirouz, M. Akbari, M. Nikkhal, *Biotechnol. Lett.* **2017**, *39*, 1279.
- [20] P. Das, S. Najafkoshnoo, J. A. Tavares-Negrete, Q. Yi, R. Esfandyarpour, *Bioprinting* **2022**, *28*, e00243.
- [21] A. Mazzocchi, S. Soker, A. Skardal, *Appl. Phys. Rev.* **2019**, *6*, 011302.
- [22] K. Joshi, V. Velasco, R. Esfandyarpour, *Sensors* **2020**, *20*, 3593.
- [23] Y. Kang, P. Datta, S. Shanmughapriya, I. T. Ozbolat, *ACS Appl. Bio Mater.* **2020**, *3*, 5552.
- [24] K. Joshi, A. Javani, J. Park, V. Velasco, B. Xu, O. Razorenova, R. Esfandyarpour, *Adv. Biosyst.* **2020**, *4*, 2000160.
- [25] J. A. Tavares-Negrete, A. E. Aceves-Colin, D. C. Rivera-Flores, G. G. Diaz-Armas, A.-S. Mertgen, P. A. Trinidad-Calderón, J. M. Olmos-Cordero, E. G. Gómez-López, E. Pérez-Carrillo, Z. J. Escobedo-Avellaneda, A. Tamayol, M. M. Alvarez, G. Trujillo-de Santiago, *ACS Biomater. Sci. Eng.* **2021**, *7*, 3964.
- [26] A. I. Frías-Sánchez, D. A. Quevedo-Moreno, M. Samandari, J. A. Tavares-Negrete, V. H. Sánchez-Rodríguez, I. González-Gamboa, F. Ponz, M. M. Alvarez, G. Trujillo-de Santiago, *Biofabrication* **2021**, *13*, 035015.
- [27] I. González-Gamboa, E. Velázquez-Lam, M. J. Lobo-Zegers, A. I. Frías-Sánchez, J. A. Tavares-Negrete, A. Monroy-Borrego, J. L. Menchaca-Arrendondo, L. Williams, P. Lunello, F. Ponz, M. M. Alvarez, G. Trujillo-de Santiago, *Front. Bioeng. Biotechnol.* **2022**, *10*, 907601.
- [28] I. Matai, G. Kaur, A. Seyedalehi, A. McClinton, C. T. Laurencin, *Biomaterials* **2020**, *226*, 119536.
- [29] J. H. Park, J. Y. Park, I.-C. Nam, M. Ahn, J. Y. Lee, S. H. Choi, S. W. Kim, D.-W. Cho, *Biomaterials* **2018**, *185*, 276.
- [30] M. Wang, W. Li, J. Hao, A. Gonzales, Z. Zhao, R. S. Flores, X. Kuang, X. Mu, T. Ching, G. Tang, Z. Luo, C. E. Garciamendez-Mijares, J. K. Sahoo, M. F. Wells, G. Niu, P. Agrawal, A. Quiñones-Hinojosa, K. Eggan, Y. S. Zhang, *Nat. Commun.* **2022**, *13*, 3317.
- [31] A. Thomas, I. Orellano, T. Lam, B. Noichl, M.-A. Geiger, A.-K. Amler, A.-E. Kreuder, C. Palmer, G. Duda, R. Lauster, L. Kloke, *Acta Biomater.* **2020**, *117*, 121.
- [32] E. Mirdamadi, J. W. Tashman, D. J. Shiwerski, R. N. Palchesko, A. W. Feinberg, *ACS Biomater. Sci. Eng.* **2020**, *6*, 6453.
- [33] Q. Yi, X. Pei, P. Das, H. Qin, S. W. Lee, R. Esfandyarpour, *Nano Energy* **2022**, *101*, 107511.
- [34] S. Najafkoshnoo, T. Kim, J. A. Tavares-Negrete, X. Pei, P. Das, S. W. Lee, J. Rajendran, R. Esfandyarpour, *Adv. Mater. Technol.* **2023**, *2201655*.
- [35] Q. Yi, S. Najafkoshnoo, P. Das, S. Noh, E. Hoang, T. Kim, R. Esfandyarpour, *Adv. Mater. Technol.* **2022**, *7*, 2101034.
- [36] T. Kim, Q. Yi, E. Hoang, R. Esfandyarpour, *Adv. Mater. Technol.* **2021**, *6*, 2001021.
- [37] S. Vanaei, M. S. Parizi, S. Vanaei, F. Saleemizadehparizi, H. R. Vanaei, *Engineered Regeneration* **2021**, *2*, 1.
- [38] T. Jiang, J. G. Munguia-Lopez, S. Flores-Torres, J. Kort-Mascort, J. M. Kinsella, *Appl. Phys. Rev.* **2019**, *6*, 011310.
- [39] Z. Wang, R. Abdulla, B. Parker, R. Samanipour, S. Ghosh, K. Kim, *Biofabrication* **2015**, *7*, 045009.
- [40] A. Urciuolo, I. Poli, L. Brandolino, P. Raffa, V. Scattolini, C. Laterza, G. G. Giobbe, E. Zambaiti, G. Selmin, M. Magnussen, L. Brigo, P. De Coppi, S. Salmasso, M. Giomo, N. Elvassore, *Nat. Biomed. Eng.* **2020**, *4*, 901.
- [41] B. E. Kelly, I. Bhattacharya, H. Heidari, M. Shusteff, C. M. Spadaccini, H. K. Taylor, *Science* **2019**, *363*, 1075.
- [42] D. Xue, Y. Wang, D. Mei, Y. Wang, S. Chen, *ACS Appl. Mater. Interfaces* **2018**, *10*, 19428.
- [43] H. Ravanbakhsh, V. Karamzadeh, G. Bao, L. Mongeau, D. Juncker, Y. S. Zhang, *Adv. Mater.* **2021**, *33*, 2104730.
- [44] Y. Lu, G. Mapili, G. Suhali, S. Chen, K. Roy, *J. Biomed. Mater. Res., Part A* **2006**, *77A*, 396.
- [45] S. V. Murphy, A. Atala, *Nat. Biotechnol.* **2014**, *32*, 773.
- [46] H. Goodarzi Hosseinabadi, E. Dogan, A. K. Miri, L. Ionov, *ACS Biomater. Sci. Eng.* **2022**, *8*, 1381.
- [47] M. Regehly, Y. Garmshausen, M. Reuter, N. F. König, E. Israel, D. P. Kelly, C.-Y. Chou, K. Koch, B. Asfari, S. Hecht, *Nature* **2020**, *588*, 620.
- [48] P. N. Bernal, P. Delrot, B. Loterie, Y. Li, J. Malda, C. Moser, R. Levato, *Adv. Mater.* **2019**, *31*, 1904209.
- [49] B. Zhang, L. Gao, Q. Xue, Z. Cui, L. Ma, H. Yang, *Bio-Des. Manuf.* **2020**, *3*, 5.
- [50] R. Rizzo, D. Ruetsche, H. Liu, M. Zenobi-Wong, *Adv. Mater.* **2021**, *33*, 2102900.
- [51] W. Li, L. S. Mille, J. A. Robledo, T. Uribe, V. Huerta, Y. S. Zhang, *Adv. Healthcare Mater.* **2020**, *9*, 2000156.
- [52] C. Thieulin, C. Pailler-Mattei, A. Abdouni, M. Djaghoul, H. Zahouani, *J. Mech. Behav. Biomed. Mater.* **2020**, *103*, 103551.
- [53] Y. Sun, Y. Zhang, Q. Wu, F. Gao, Y. Wei, Y. Ma, W. Jiang, K. Dai, *Theranostics* **2021**, *11*, 5160.
- [54] Y. Chen, C. Guo, E. Manousiouthakis, X. Wang, D. M. Cairns, T. T. Roh, C. Du, D. L. Kaplan, *Adv. Funct. Mater.* **2020**, *30*, 2000543.

- [55] A. Pardo, S. M. Bakht, M. Gomez-Florit, R. Rial, R. F. Monteiro, S. P. B. Teixeira, P. Taboada, R. L. Reis, R. M. A. Domingues, M. E. Gomes, *Adv. Funct. Mater.* **2022**, 2208940.
- [56] S. K. Kalyoncu, Y. Huang, Q. Song, O. Boyraz, *Opt. Express* **2012**, *20*, 27542.
- [57] S. K. Kalyoncu, Y. Huang, Q. Song, O. Boyraz, *IEEE Photonics J.* **2013**, *5*, 5500207.
- [58] X. Xiao, X. Dong, Y. Yu, *Opt. Express* **2021**, *29*, 33785.
- [59] B. Smith, B. Hellman, A. Gin, A. Espinoza, Y. Takashima, *Frontiers in Optics 2017*, OSA, Washington, D.C. **2017**, pp. 89–94.
- [60] Y. Huang, Q. Zhao, S. K. Kalyoncu, R. Torun, Y. Lu, F. Capolino, O. Boyraz, *Appl. Phys. Lett.* **2014**, *104*, 161106.
- [61] S. K. Kalyoncu, R. Torun, Y. Huang, Q. Zhao, O. Boyraz, *J. Micro Nano-Manuf.* **2014**, *2*, 021004.
- [62] DLP Texas Instruments, DLP 0.55XGA Chipset, **2022**. <https://www.ti.com/lit/ds/symlink/dlp5500.pdf?ts=1677697843579>
- [63] M. A. Cox, in *Complex Light and Optical Forces XIV*, (Eds: D. L. Andrews, E. J. Galvez, H. Rubinsztein-Dunlop), SPIE, Bellingham, WA **2021**, p. 44.
- [64] B. D. Fairbanks, M. P. Schwartz, C. N. Bowman, K. S. Anseth, *Biomaterials* **2009**, *30*, 6702.
- [65] X. Ma, X. Qu, W. Zhu, Y.-S. Li, S. Yuan, H. Zhang, J. Liu, P. Wang, C. S. E. Lai, F. Zanella, G.-S. Feng, F. Sheikh, S. Chien, S. Chen, *Proc. Natl. Acad. Sci. U. S. A.* **2016**, *113*, 2206.
- [66] A. Shapira, T. Dvir, *Adv. Sci.* **2021**, *8*, 2003751.
- [67] D. Ortolan, R. Sharma, A. Volkov, A. Maminishkis, N. A. Hotaling, L. A. Huryh, C. Cukras, S. Di Marco, S. Bisti, K. Bharti, *Proc. Natl. Acad. Sci. U. S. A.* **2022**, *119*, e2117553119.
- [68] H. Nam, H.-J. Jeong, Y. Jo, J. Y. Lee, D.-H. Ha, J. H. Kim, J. H. Chung, Y.-S. Cho, D.-W. Cho, S.-J. Lee, J. Jang, *Sci. Rep.* **2020**, *10*, 7255.
- [69] L. Yao, W. Daly, B. Newland, S. Yao, W. Wang, B. K. K. Chen, N. Madigan, A. Windebank, A. Pandit, *Gene Ther.* **2013**, *20*, 1149.
- [70] J. H. Lee, R. K. Prud'homme, I. A. Aksay, *J. Mater. Res.* **2001**, *16*, 3536.
- [71] W. Stopyra, J. Kurzac, K. Gruber, T. Kurzynowski, E. Chlebus, In *Laser Technology 2016: Progress and Applications of Lasers*, Vol. 10159, SPIE, **2016**, pp. 240–246.
- [72] S. Yeleswarapu, S. Chameettachal, F. Pati, *ACS Appl. Bio Mater.* **2021**, *4*, 6982.
- [73] M. Zanon, D. Baruffaldi, M. Sangermano, C. F. Pirri, F. Frascella, A. Chiappone, *Eur. Polym. J.* **2021**, *160*, 110813.
- [74] H. Atcha, A. Jairaman, J. R. Holt, V. S. Meli, R. R. Nagalla, P. K. Veerasubramanian, K. T. Brumm, H. E. Lim, S. Othy, M. D. Cahalan, M. M. Pathak, W. F. Liu, *Nat. Commun.* **2021**, *12*, 3256.
- [75] C. B. Hutson, J. W. Nichol, H. Aubin, H. Bae, S. Yamanlar, S. Al-Haque, S. T. Koshy, A. Khademhosseini, *Tissue Eng., Part A* **2011**, *17*, 1713.
- [76] A. Bandyopadhyay, B. B. Mandal, N. Bhardwaj, *J. Biomed. Mater. Res., Part A* **2022**, *110*, 884.
- [77] A. Tong, Q. L. Pham, P. Abatemarco, A. Mathew, D. Gupta, S. Iyer, R. Voronov, *SLAS Technol.* **2021**, *26*, 333.
- [78] N. A. Peppas, J. Z. Hilt, A. Khademhosseini, R. Langer, *Adv. Mater.* **2006**, *18*, 1345.
- [79] A. A. Weiner, D. M. Shuck, J. R. Bush, V. P. Shastri, *Biomaterials* **2007**, *28*, 5259.
- [80] K. Yue, G. Trujillo-de Santiago, M. M. Alvarez, A. Tamayol, N. Annabi, A. Khademhosseini, *Biomaterials* **2015**, *73*, 254.
- [81] J. J. Schwartz, A. J. Boydston, *Nat. Commun.* **2019**, *10*, 791.
- [82] T. J. Hinton, A. Hudson, K. Pusch, A. Lee, A. W. Feinberg, *ACS Biomater. Sci. Eng.* **2016**, *2*, 1781.
- [83] Y. Jin, A. Compaan, T. Bhattacharjee, Y. Huang, *Biofabrication* **2016**, *8*, 025016.